

Global autocorrelation scales of the partial pressure of oceanic CO₂

Zhen Li

Science Applications International Corporation/General Sciences Corporation, Beltsville, Maryland, USA

David Adamec

Oceans Sciences Branch, NASA Goddard Space Flight Center, Greenbelt, Maryland, USA

Taro Takahashi and Stewart C. Sutherland

Lamont-Doherty Earth Observatory of Columbia University, Palisades, New York, USA

Received 22 September 2004; revised 18 March 2005; accepted 20 April 2005; published 4 August 2005.

[1] A global database of approximately 1.7 million observations of the partial pressure of carbon dioxide in surface ocean waters ($p\text{CO}_2$) collected between 1970 and 2003 is used to estimate its spatial autocorrelation structure. The patterns of the lag distance where the autocorrelation exceeds 0.8 is similar to patterns in the spatial distribution of the first baroclinic Rossby radius of deformation indicating that ocean circulation processes play a significant role in determining the spatial variability of $p\text{CO}_2$. Separate calculations for times when the Sun is north and south of the equator revealed no obvious seasonal dependence of the spatial autocorrelation scales. The $p\text{CO}_2$ measurements at Ocean Weather Station (OWS) "P" in the eastern subarctic Pacific (50°N, 145°W) is the only fixed location where an uninterrupted time series of sufficient length exists to calculate a meaningful temporal autocorrelation function for lags greater than a few days. The estimated temporal autocorrelation function at OWS "P" is highly variable. A spectral analysis of the longest four $p\text{CO}_2$ time series indicates a high level of variability occurring over periods from the atmospheric synoptic to the maximum length of the time series, in this case 42 days. It is likely that a relative peak in variability with a period of 3–6 days is related to atmospheric synoptic period variability and ocean mixing events due to wind stirring. However, the short length of available time series makes identifying temporal relationships between $p\text{CO}_2$ and atmospheric or ocean processes problematic.

Citation: Li, Z., D. Adamec, T. Takahashi, and S. C. Sutherland (2005), Global autocorrelation scales of the partial pressure of oceanic CO₂, *J. Geophys. Res.*, 110, C08002, doi:10.1029/2004JC002723.

1. Introduction

[2] The partial pressure of CO₂ ($p\text{CO}_2$) in seawater is a vapor pressure of CO₂, and hence governs the magnitude of the CO₂ transfer flux across the sea-air interface when multiplied with sea-air gas transfer coefficient. It is a sensitive function of temperature doubling with every 16°C [Takahashi *et al.*, 1993]. It is also a sensitive function of the total concentration of CO₂ (TCO₂) species dissolved in seawater,

$$\text{TCO}_2 = [\text{CO}_2]_{\text{aqueous}} + \text{HCO}_3^- + \text{CO}_3^{--},$$

that depends on the net biological community production, the rate of upwelling of subsurface waters rich in CO₂, and the air-sea CO₂ flux. The local sensitivity may be expressed in terms of the Revelle factor, $\frac{\partial \ln p\text{CO}_2}{\partial \ln \text{TCO}_2}$, which varies from 8 with lower TCO₂ concentrations in tropical waters to 15

with higher concentrations in polar waters. In the surface mixed layer, the effect of warming on $p\text{CO}_2$ is counteracted by lower TCO₂ caused by photosynthetic fixation of CO₂, as often seen during spring bloom periods, and the effect of cooling is counteracted by increasing TCO₂ usually caused by upwelling of subsurface waters rich in respired CO₂. Consider the following example. A parcel of polar ocean water at -1.9°C warmed to an equatorial temperature of 30°C without changes in TCO₂ and other chemicals, increases its $p\text{CO}_2$ by a factor of 4. If the typical nitrate in this water (~35 μmol/kg) is completely utilized by biological growth with the Redfield N/C ratio of 16/106, then the TCO₂ in the same water would decrease from 2150 μmol/kg to 1920 μmol/kg. Thus there is a decrease in $p\text{CO}_2$ by a factor of $(1920/2150)^{10} \approx 33\%$ (using a Revelle factor of 10). This example illustrates that over the global oceans, the effect of change in temperature is roughly compensated by changes in TCO₂, and that the time-space variation in surface seawater $p\text{CO}_2$ is dictated primarily by interactions between the effects of temperature, net biological production, and the deep water upwelling rate. Using climatological mean data, Takahashi *et al.* [2002]

have observed that in subtropical gyres, seasonal changes in $p\text{CO}_2$ are due primarily to temperature changes, whereas those in subpolar and polar waters are due primarily to TCO_2 changes caused by winter upwelling of subsurface waters and spring plankton blooms in spring. However, finer scale time-space variability of surface water $p\text{CO}_2$ has not been investigated using semi-continuous underway surface water $p\text{CO}_2$ measurements which have been made in increasing numbers during recent years.

[3] In this study, the global distribution of the isotropic spatial autocorrelation structure of available $p\text{CO}_2$ underway measurements is calculated. The approach taken is similar to that of *Murphy et al.* [2001], who investigated $p\text{CO}_2$ autocorrelation structure in the Bering Sea. The motivation is to identify the scales of variability that are resolved in the $p\text{CO}_2$ data, and attempt to relate some of that variability to known physical processes. In addition, time series data available from OWS "P" is similarly analyzed to provide an example of temporal autocorrelation structure and variability. It is hoped that a quantified estimate of autocorrelation scales will be useful to investigators, particularly future data assimilation efforts, for decisions on how best to use the 1.7 million measurements in choosing averaging and subsampling schemes for their work.

2. Data

[4] For the global studies, most of the $p\text{CO}_2$ measurements in surface mixed layer waters (hereinafter referred to simply as $p\text{CO}_2$) are mostly composed of underway ship-board measurements and a much smaller number of measurements for discrete water samples collected at hydrographic stations. The underway data used for both *Takahashi et al.* [1997, 2002] studies was temporally averaged to 12-hourly intervals, the averaging reducing the number of total observations as underway measurements in the complete data set are sometimes taken as frequently as every 2 min, but usually several times per hour. The 12-hourly (approximately 100 km) averaging period was chosen ostensibly to maintain the larger scale gradient structure of $p\text{CO}_2$ in the total data set.

[5] While the raw number of $p\text{CO}_2$ measurements (currently approaching 1.7 million in some data sets) may seem adequate, or perhaps even large, for global studies, the number of actual data values used in past studies is much lower because of the averaging of the underway data as noted above. Even the choice of averaging period/distance is, in some ways, an ad hoc choice depending on the scales of interest and the accuracy of underway data versus station point data. Indeed, the relative paucity of accurate $p\text{CO}_2$ measurements has led some investigators to try to infer $p\text{CO}_2$ values from other properties of the seawater, such as temperature. For example, *Boutin et al.* [1999], *Cosca et al.* [2003], and *Feely et al.* [2004] found strong covariability between $p\text{CO}_2$ and sea surface temperature in the equatorial Pacific, and *Loukos et al.* [2000] were able to show a useful predictive skill of temperature and salinity for TCO_2 in the equatorial Pacific.

[6] The $p\text{CO}_2$ data used here is an expanded version of the data used by *Takahashi et al.* [2002], including about 760,000 new observations bringing the total to approximately 1.7 million. The data was collected between 1970

and 2003, and its geographic and rough temporal distributions are shown in Figure 1. Note that, for the most part, the entire Indian and South Pacific Oceans are only sparsely sampled prior to 1990. Much of the sampling in the South Atlantic occurred between 1985 and 1989. Prior to 1985, the only sub-basin that is sampled more densely is the North Atlantic. A caution on the results presented here is that the results apply to sampling that primarily took place post 1984.

[7] All autocorrelation calculations are performed on data interpolated to regularly spaced segments with a distance of 2 km between successive data points. Interpolating $p\text{CO}_2$ data across gaps larger than 20 km is not done. For gaps larger than 20 km, a new segment is defined. Also, interpolation across a gap in time of longer than 10 days is not allowed, and a new segment would be defined. This latter condition was very rarely met. Average autocorrelation functions are calculated globally on a $10^\circ \times 10^\circ$ grid. The location of the segment is taken to be the average latitude and longitude of the measurement locations. Segments shorter than 60 km were not included in the calculations, and no single segment was allowed to exceed 1000 km, approximately the length of the grid box. For segments longer than 1000 km, a group of subsegments, broken every 1000 km, was used for the calculations. Thus the autocorrelations describe variability on approximate spatial scales less than the grid box resolution.

[8] The global distribution of segments is not homogeneous, and the number of segments in each grid box is presented in Figure 2. Areas of densest coverage include the tropical Pacific, the North Pacific near the coast of Japan and north of 45°N , the northwest Indian Ocean, the Caribbean, and specific locales in the Southern Ocean. In many places, the correlations presented are the result from only one or two segments, such as is the case for much of the South Atlantic and Pacific Oceans. In those areas, little confidence can be placed in the autocorrelation structure, but they are nevertheless presented for completeness.

[9] In addition to the global 10° grid, seven ocean-relevant areal averages of autocorrelation functions are presented. Those areas include: the Kuroshio subtropical gyre, 135°E – 180°E , 25°N – 40°N ; eastern equatorial Pacific, 180°E – 80°W , 10°S – 10°N ; northeast Pacific, 150°W – 120°W , 30°N – 50°N ; East Australia gyre, 150°E – 180°E , 40°S – 10°S ; Gulf Stream subtropical gyre, 80°W – 50°W , 25°N – 40°N ; North Atlantic subpolar gyre, 60°W – 10°W , 40°N – 60°N ; and the tropical Indian, 30°E – 100°E , 20°S – 10°N .

3. Spatial Autocorrelation Structure

[10] The lag autocorrelation function, $AC(\text{lag})$, is calculated as follows:

$$AC(\text{lag}) = \frac{\sum_{i=0}^{N-\text{lag}} (x_i - \bar{x})(x_{i+\text{lag}} - \bar{x})}{\sum_{i=0}^{N-\text{lag}} (x_i - \bar{x})^2},$$

where x is the measurement value and an overbar represents the average value. The spatial distance of the lag is simply the product of the index lag times the grid resolution between consecutive data points, in this case, 2 km. For this study, we present results for an isotropic

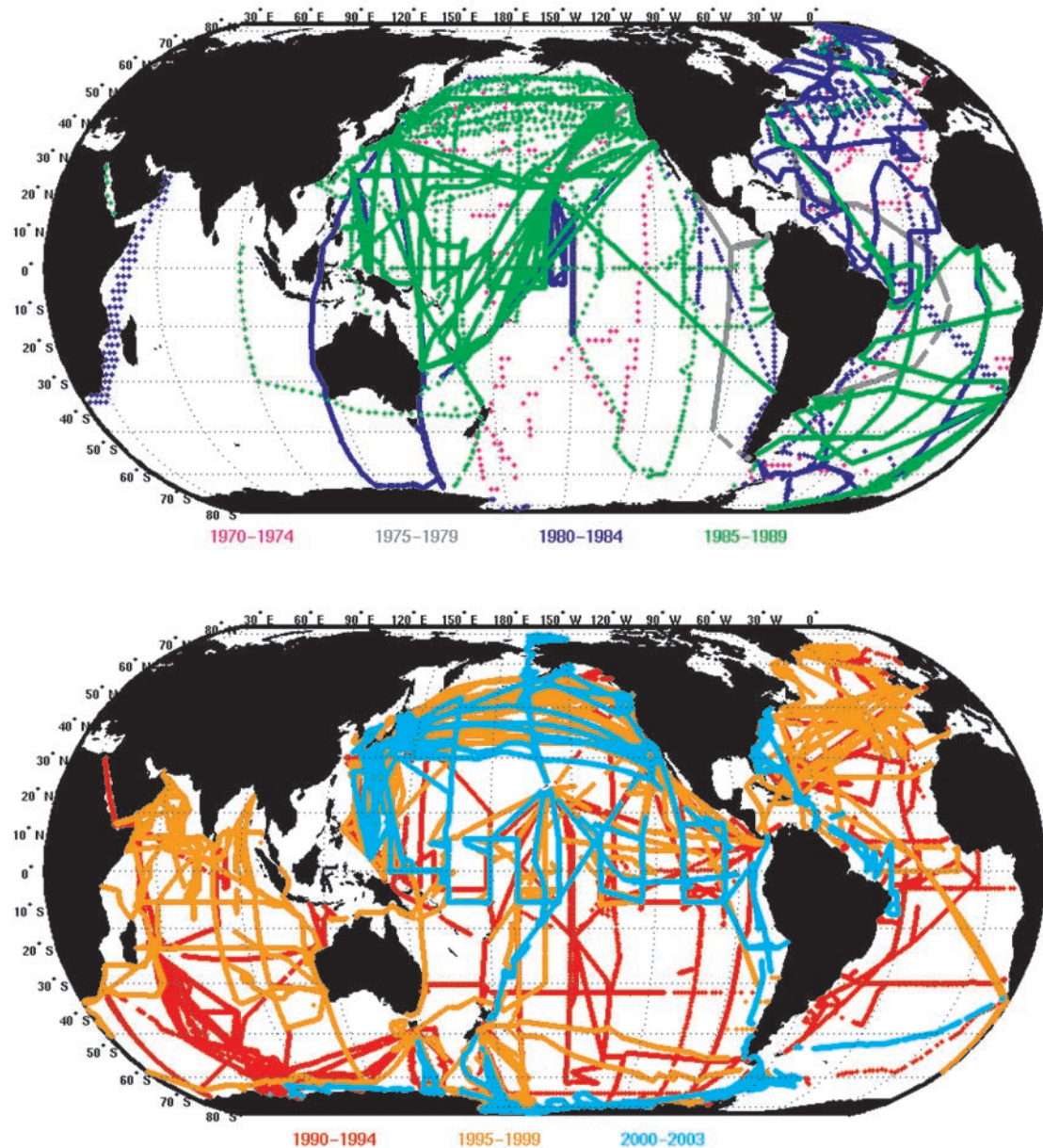


Figure 1. Spatial and temporal distributions of ocean surface $p\text{CO}_2$ measurements taken between 1970 and 2003. The location is marked on the map by a colored marker. The color of the marker indicates the pentad during which the observation was taken.

autocorrelation only, understanding that there are locations where the autocorrelation function is almost certainly not isotropic, near 40°N – 45°N in the North Pacific, for example. *Murphy et al.* [2001] performed identical calculations for 24 basin long repeat tracks of $p\text{CO}_2$ measurements made over a 48-month period along nearly great circle routes in the North Pacific. That study concentrated on the large-scale spatial decorrelation estimates, and found that $p\text{CO}_2$ data became completely decorrelated ($\text{AC} = 0$) at about 1.5° longitude (105 km along the east-west direction) in the Bering Sea and 3.5° longitude (250 km along the NW-SE direction) in the Gulf of Alaska. In this study, it is the smaller scale variability that is of interest, and many data segments are not of sufficient length to allow AC to approach 0.

[11] The significance of the calculated spatial AC is naturally dependent on the number of input data points to the AC calculation. A typical segment in this study consists of about 400 data points. Using a Student-T test criterion, only AC exceeding 0.1 is significant at the 95% confidence limit. For the worst case scenario of 30 data points, any AC exceeding 0.51 is significant at the 95% confidence limit.

[12] Rather than presenting an estimate of the spatial autocorrelation function for each grid box, the global structure is presented as the lag distance at which the autocorrelation estimate drops below a specific value. The first map (Figure 3a) indicates the distance over which the autocorrelation is termed high, here, greater or equal to 0.8. The second map is the distance over which the autocorrelation is termed elevated, 0.6. Both the 0.8 and 0.6

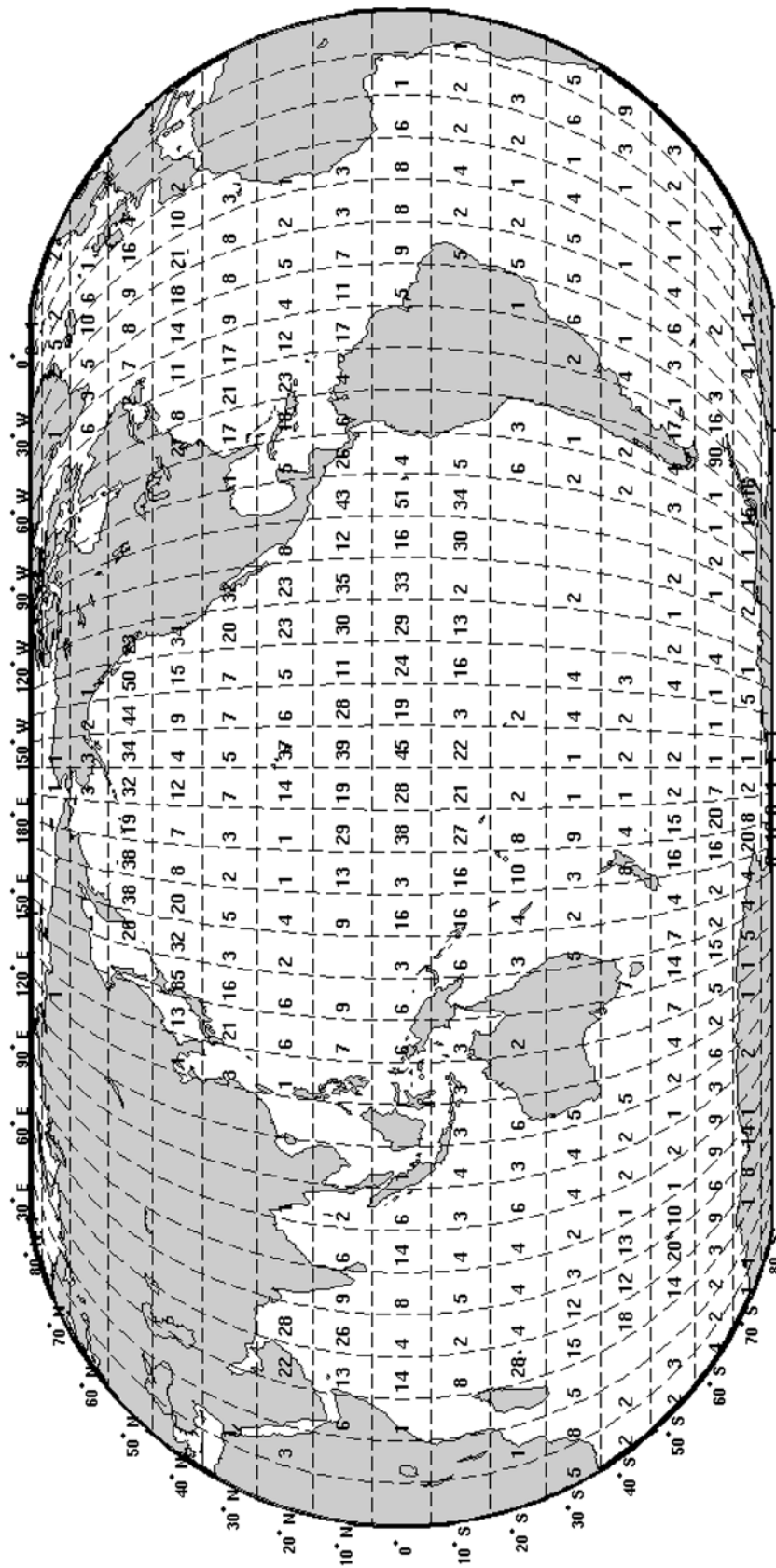


Figure 2. Distribution of the total number of defined $p\text{CO}_2$ measurement segments within each $10^\circ \times 10^\circ$ box. Empty boxes contain no $p\text{CO}_2$ measurements.

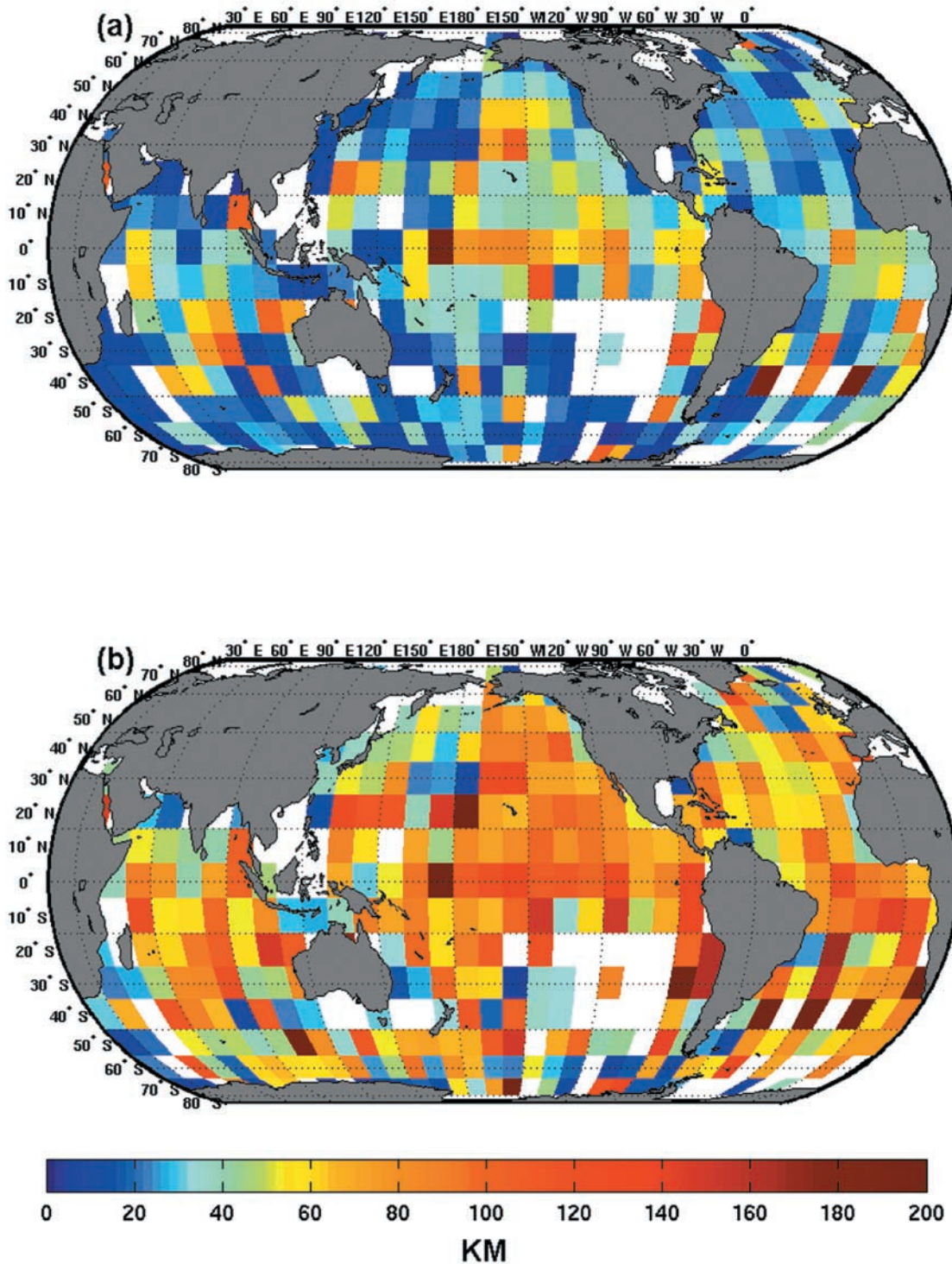


Figure 3. (a) Global distribution of lag distance where the spatial autocorrelation exceeds 0.8, and (b) the lag distance where the spatial autocorrelation exceeds 0.6.

values of AC are always significant at the 95% confidence limit. These definitions of high and elevated are arbitrary but nevertheless convenient for discussion purposes. The statistical significance of each autocorrelation is a function proportional to the number of data points that enter into the calculation of AC and varies geographically in this study (see Figure 2). The globally recognizable feature is that the

lag distance is shorter in high-latitude areas and increases toward the equator, consistent with the dependence of the Rossby radius of deformation on the inverse of the local Coriolis acceleration.

[13] The largest area where high autocorrelations extend to the greatest distance is in the immediate vicinity of the equatorial Pacific where that distance is routinely greater

than 80 km, ranging from 100 km to 250 km. There is some indication this “high correlation distance” is greater north of the equator than it is to the south in the Pacific Ocean. In the Atlantic, the high correlation distance is greater north of the equator than it is directly on the equator. In the Indian Ocean, the high correlation distance is greater south of the equator than it is to the north of the equator. The asymmetry in the Indian Ocean may be due to the long annual Rossby waves that dominate much of the variability in the southern Indian Ocean but does not in the north.

[14] In the Northern Hemisphere subtropical gyres, the distance is greater (about 50 km) in the Atlantic compared to the Pacific where the distance is below 30 km. This distribution would be consistent with the eddy transfer scales in these gyres as the internal deformation radius of the subtropical gyre in the Atlantic is about 45 km, and the deformation radius is about 25 km in the Pacific (see *Emery et al.* [1984] for estimates of deformation radii based on local vertical Brunt-Väisälä profiles). At high latitudes, the high correlation distance is 20 km and shorter, consistent again with the smaller deformation radii at these latitudes. Thus, in general, the distance for autocorrelations greater than 0.8 is consistent with scales set by the physical properties of the ocean flow in many areas.

[15] Not surprisingly, there are aspects of the elevated autocorrelation distance (Figure 3b) that are similar to the patterns of high correlation distance. For example, the longest distance for elevated autocorrelations is in the equatorial Pacific. Also, there are longer distances for elevated autocorrelation in the Gulf Stream gyre compared to the Kuroshio subtropical gyre as in the high correlation distance pattern. However, there are areas in the high latitudes that have elevated autocorrelation distance that are comparable to the distances in the subtropics. This is somewhat evident in both the North Atlantic and North Pacific, indicating the autocorrelation function does not have a steep drop between 0.8 and 0.6 in those areas. Also note that the distances with elevated correlation are longer in the Gulf of Alaska compared to those east of the dateline at the same latitude consistent with the calculations of *Murphy et al.* [2001].

[16] It is worth noting that even though the *Murphy et al.* [2001] study and this study used differing resolutions for the input data (10 km versus 2 km for the present study), both studies seemingly arrive at the same lag distance over which the autocorrelation drops below 0.8 in the northern North Pacific, about 20–40 km. However, the same zonal asymmetry appearing in both studies is a little surprising. The data used by *Murphy et al.* [2001] for the northernmost tracks between 170°E and 165°W were restricted within the Bering Sea, and the $p\text{CO}_2$ variability may likely reflect local turbulence generated by the Aleutian Island chain. In contrast, the variability of the northern North Pacific in our study is represented mainly by data south of the island chain in the open North Pacific. Here the shortened autocorrelation scales seem more likely tied to the variability of the Kuroshio Extension and Oyashio as opposed to local island effects that may have been important in the analysis of *Murphy et al.* [2001].

[17] Around the Antarctic Circumpolar Current, the situation is more complex, and changes in the elevated auto-

correlation distance often vary greatly in adjacent grid boxes. The variability in this region is controlled by a strongly meandering zonal flow. The spatial scale of the local variability is much smaller than the $10^\circ \times 10^\circ$ box used in this study. Thus the Antarctic Circumpolar Current and its variability are very much undersampled, and this may explain the strong box-to-box variability in the autocorrelation calculations presented here.

[18] The same calculations were repeated, except that average autocorrelation structures were calculated for two seasons, March–August and September–February, when the Sun is at maximum zenith in the Northern and Southern Hemisphere, respectively. Except for a slight tendency for there to be longer autocorrelation distances in the subtropical gyres when the Sun is at zenith in the local hemisphere, there is very little seasonal change with the calculated autocorrelation structure. The change in the subtropical gyres was not significant enough to warrant showing the figures for the seasonal changes. The rapid change in autocorrelation structure over relatively short distances near the Antarctic Circumpolar Current did not change with season. Thus biology seems an unlikely candidate for a single controlling factor of this spatial behavior. This is consistent with the small seasonal amplitudes of $p\text{CO}_2$ observed in the 40°S–60°S zone suggesting that $p\text{CO}_2$ changes due to SST are largely compensated by changes in TCO_2 due to the biological utilization and upwelling [*Takahashi et al.*, 2002]. The highly variable current and wind forcing make it difficult to assign any one reason for such variability in this area of strong horizontal and vertical mixing.

[19] Figure 4 is the estimated autocorrelation structure for seven specific geographic areas defined in the DATA section of this manuscript. Along with the estimated structure, a least squares best fit exponential curve to the average autocorrelation function is given to provide an estimate of an exponential decay scale of this structure. As indicated by the $10^\circ \times 10^\circ$ estimates, the equatorial Pacific has the longest exponential decay scale of about 139 km. Also, the Gulf Stream decorrelation scale is nearly double that which occurs near the Kuroshio. An unexpected result is the relatively long 92 km e-folding scale in the North Atlantic subpolar gyre. Note, however, that the drop-off for the highest correlation scales is not represented well by the best fit line in this area and a simple exponential decay would be an obviously poor choice for a functional representation of the autocorrelation function. This is also the case in the East Australia current region. Note that there is no reason to expect that the AC function should be well represented by a simple exponential decay. Indeed, many physical variables are not well represented by such a function [e.g., *Rienecker et al.*, 1987]. The reason for providing an exponential estimate is for a globally consistent basis for comparison. Caution is advised for detailed comparisons where the AC does not seem to follow a simple exponential decay.

4. Temporal Autocorrelation Structure

[20] Within this $p\text{CO}_2$ database, there are but a few time series of sufficient length to conduct meaningful temporal autocorrelation analysis. The $p\text{CO}_2$ time series at Hydrostation “S” (32°10′N, 64°30′W) and Bermuda Atlantic

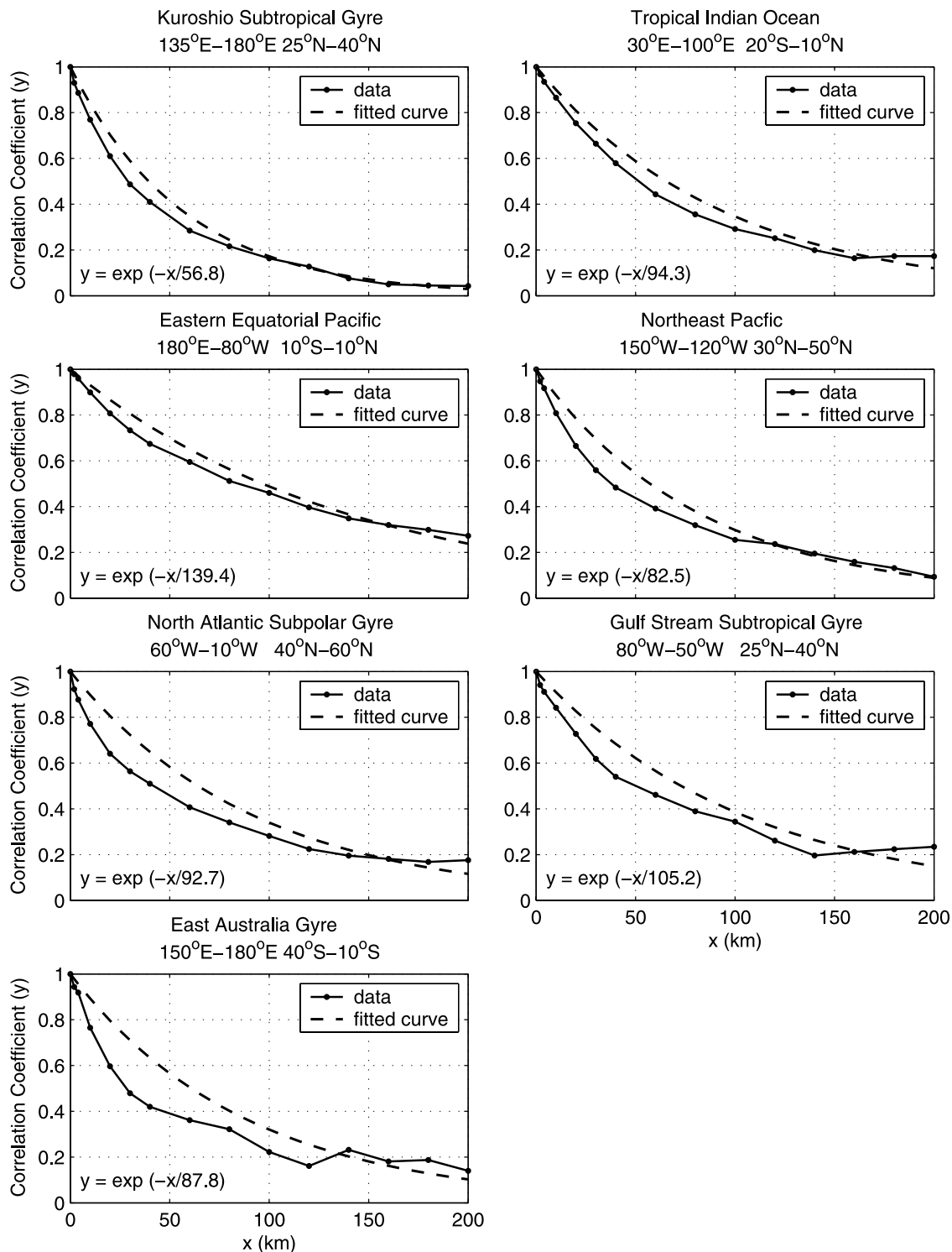


Figure 4. Estimated average spatial autocorrelation functions for seven specific geographic locations (solid lines with circles) and their best fits (dashed lines) assuming an exponential decay scale.

Time Series Study (BATS) site (31°50'N, 64°10'W) [Bates *et al.*, 1998] in the Sargasso Sea, did not contain an uninterrupted time series longer than a few days. Much of the temporal analysis previously done for OWS “P” used, at best, weekly averaged data. For example, Wong and Chan [1991] analyzed the seasonal variation of $p\text{CO}_2$ at OWS

“P” using monthly and weekly averaged values of $p\text{CO}_2$ and reported slightly higher values of $p\text{CO}_2$ during summer compared to winter. Here the emphasis is on detailed temporal autocorrelation structure.

[21] The temporal autocorrelation structure for the 11 longest uninterrupted time series from OWS “P” are

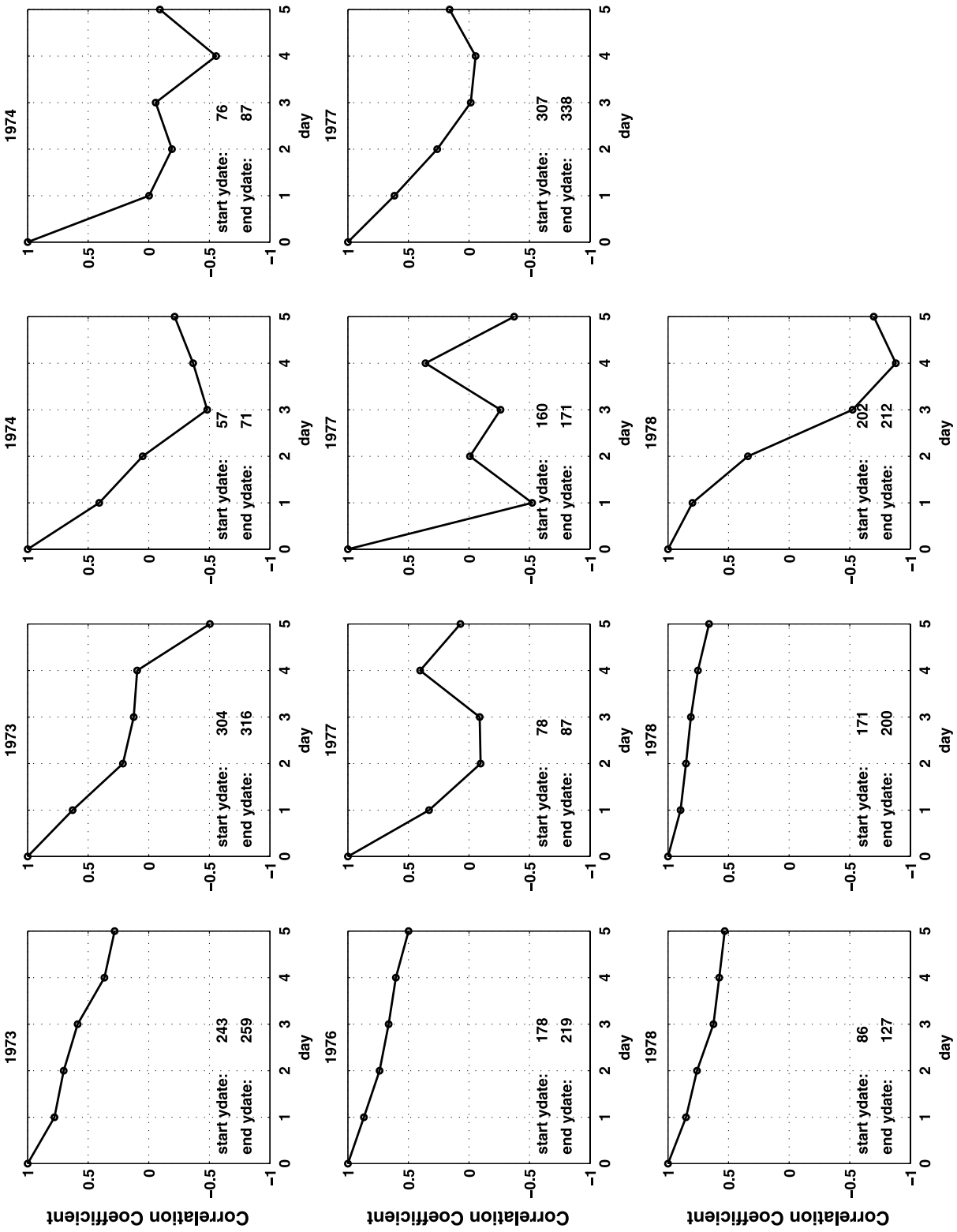


Figure 5

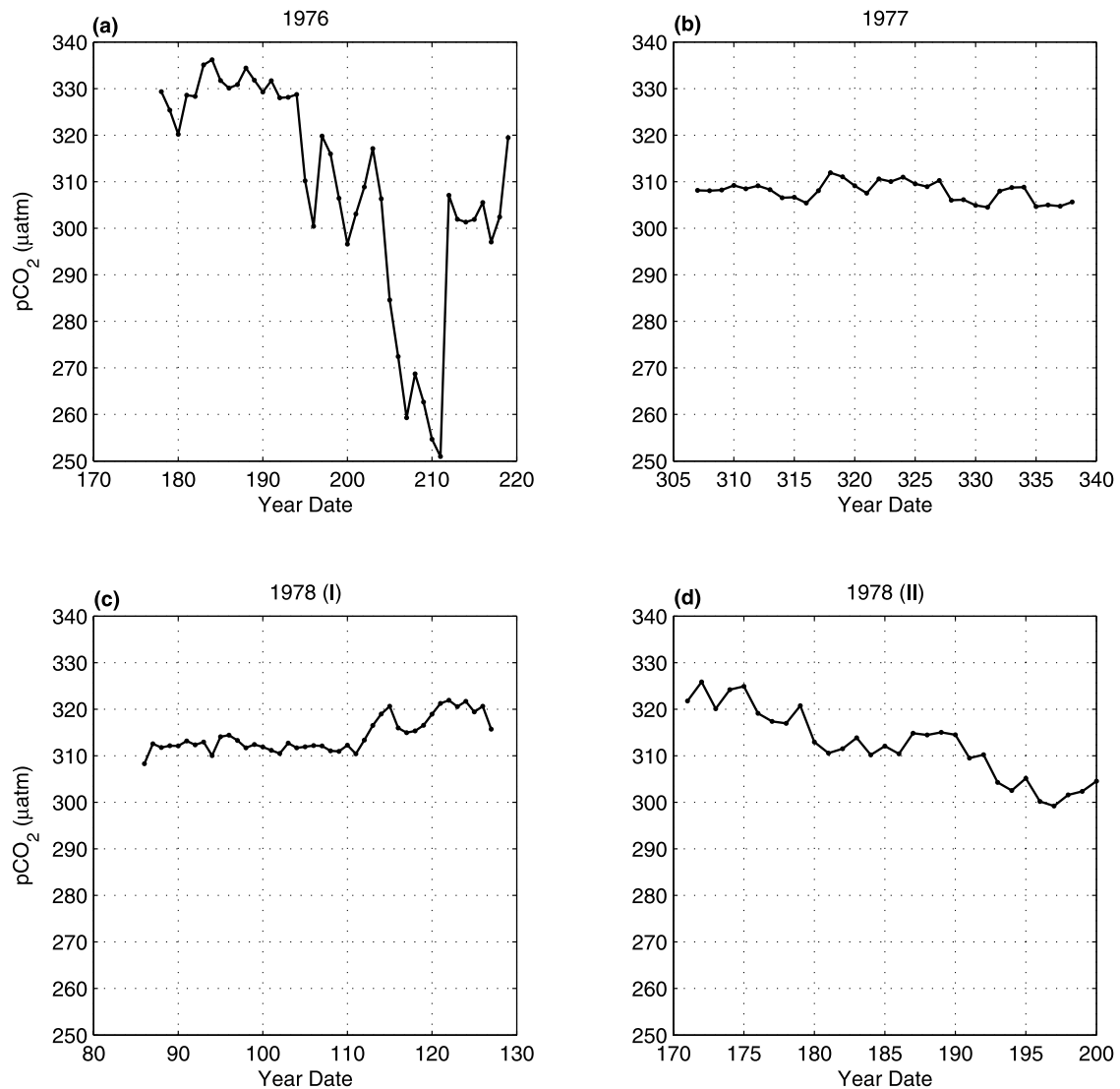


Figure 6. Four longest time series of daily averaged $p\text{CO}_2$ from Ocean Weather Station (OWS) “P” in the eastern subarctic Pacific (50°N , 145°W). These $p\text{CO}_2$ series are chosen for display because the length of each time series is at least 30 days. The year of observation is shown above each plot, and the Julian Day is marked on the abscissa.

shown in Figure 5. The 6-hourly reported data have been averaged to daily values to remove diurnal effects. All these time series are from the 1970s with the longest segment being 42 days during 1978. Others are as short as 10 days. The shorter segments obviously have less confidence associated with the estimated structure. For the shorter segments, only AC exceeding 0.6 are significant at the 95% level. For the longer temporal segment, AC exceeding 0.38 are significant. Whereas there are instances where the autocorrelation coefficient remains relatively high after a 5-day lag, the longer decorrelation scales can really not be associated with any particular time of year. The last two structures for

the summer of 1978 illustrate this point. Whereas for Julian days 171–200 during 1978 the autocorrelation coefficient at 5-day lag is about 0.6, immediately following for Julian days 202–212, the coefficient is near 0 between 2 and 3 day lags. From the data available, it is difficult to assign a general structure to the temporal autocorrelation structure of daily $p\text{CO}_2$, even for a particular season. It is possible that longer period averaging, say weekly or monthly, might produce more consistent autocorrelation structure; however, the available data cannot support those calculations.

[22] Because uninterrupted time series of oceanic $p\text{CO}_2$ are scarce, an attempt is made to use other variables as a

Figure 5. Estimates of the temporal autocorrelation structure for the 11 longest uninterrupted time series from Ocean Weather Station (OWS) “P” in the eastern subarctic Pacific (50°N , 145°W). The year of observation is shown above each plot, and the Julian Day of the beginning and end of each series is labeled within the plot.

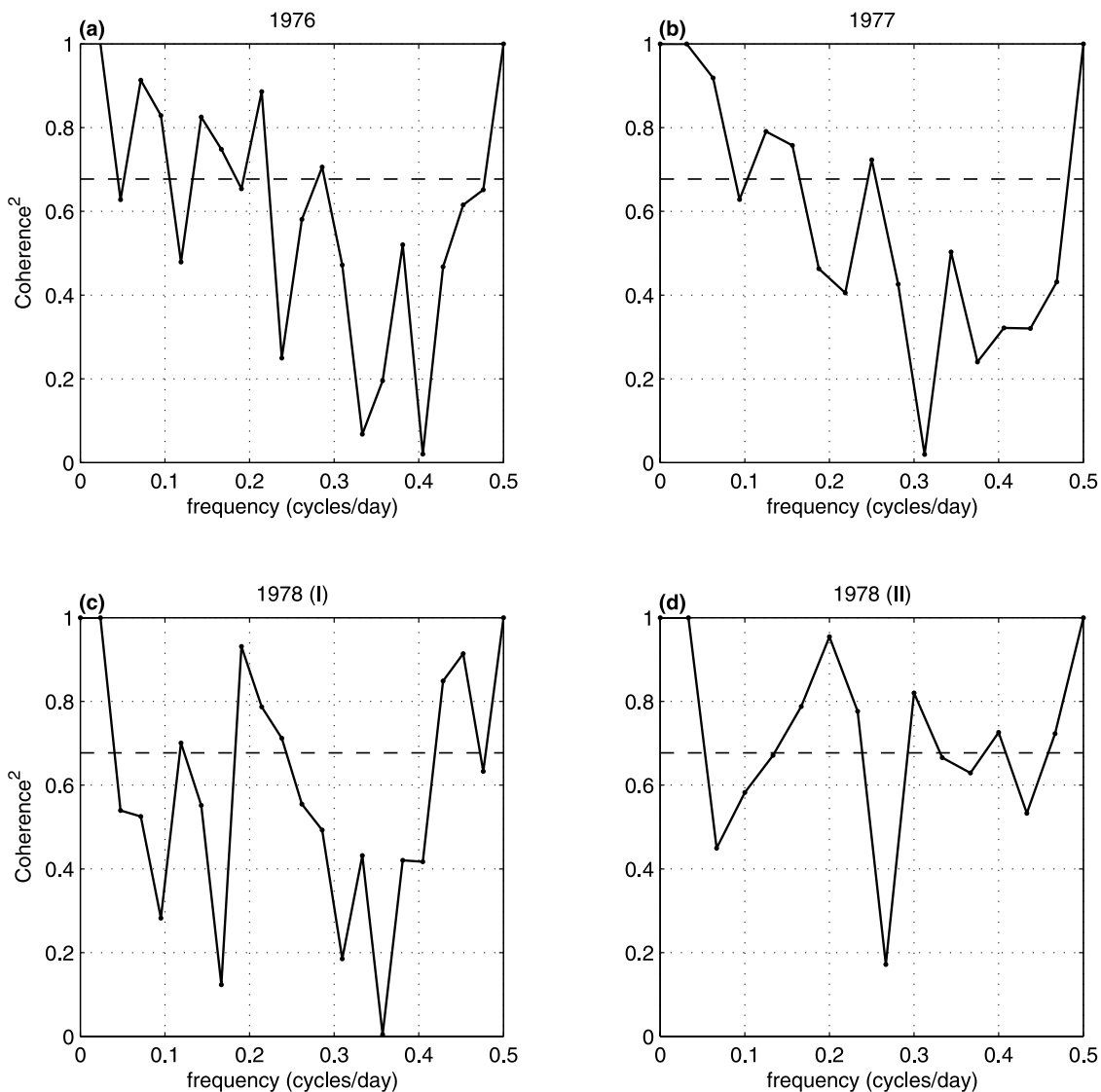


Figure 7. Coherence spectra between temperature and $p\text{CO}_2$ for the four time periods shown in Figure 6. The coherence was estimated using a Hanning (1-2-1) filter on both the Fourier transforms and the auto- and cross-spectral estimates. The associated 95% significance level (dashed lines) on coherence squared is 0.67.

proxy to estimate the $p\text{CO}_2$ correlation structure, specifically temperature because of the great sensitivity of $p\text{CO}_2$ to temperature. *Boutin et al.* [1999] and *Cosca et al.* [2003] found that some of the $p\text{CO}_2$ variability in the eastern equatorial Pacific could be explained by the variability in temperature. Here the four time series with $p\text{CO}_2$ data for at least 30 uninterrupted days is used to investigate the co-variability of $p\text{CO}_2$ with temperature and salinity. The four $p\text{CO}_2$ time series are shown in Figure 6. As in the work of *Wong and Chan* [1991], most of the values of $p\text{CO}_2$ are between 290 and 340 μatm . The exception occurred during the summer of 1976 when a likely mixing event dropped surface $p\text{CO}_2$ values to near 250 μatm . The temperature and salinity data for this period show no unusual behavior. Since no nutrient concentration data are available for this period, the low $p\text{CO}_2$ values cannot be attributed unequivocally to biological utilization of CO_2 .

[23] Rather than presenting a simple correlation, we choose to present the coherence spectra between the temperature and $p\text{CO}_2$ data. The data are detrended by removing a linear best fit line, likely removing most of any local seasonal signal. The estimate of coherence between variables is identical to unity except when smoothing is applied to the estimates of the Fourier transforms and the auto and cross spectra. For this analysis, a simple Hanning smoother, where a spectral component is replaced with a weighted (1-2-1) average of its surrounding components, is applied twice. The coherence spectra for the four time periods between temperature and $p\text{CO}_2$ are shown in Figure 7. The value of coherence being 1 at either side of the frequency extremes is owing to no smoothing of the spectra at end points. For the limited number of input data and Fourier smoothing applied, only coherences above 0.67 are significant at the 95% confidence limit.

[24] The jaggedness in each of the coherence spectra is obvious. Whereas the 1976 and 1977 periods might indicate greater coherence at lower frequencies, the 1978 sequences do not. Except for the 1977 series, there is a local peak at 0.2 cycles per day that might indicate that $p\text{CO}_2$ variability is related to mixing forced by atmospheric synoptic variability. However, it is difficult to say that a clear picture of covariability between $p\text{CO}_2$ and temperature on any particular timescale. Although not presented, the results are no more clear for $p\text{CO}_2$ and salinity covariability than they are for $p\text{CO}_2$ and temperature covariability at OWS "P."

[25] The seasonal variability of $p\text{CO}_2$ observed in the OWS "P" area is generally less than 30 μatm (with an exception of one event in the summer of 1976) as shown in Figure 6. This is about 20% of 140 μatm that is expected from the 9°C seasonal SST changes if no change in TCO_2 occurred ($\partial \ln p\text{CO}_2/\partial T = 0.0423^\circ\text{C}^{-1}$). Takahashi *et al.* [2002] have shown that the temperature effect was largely cancelled by the biological drawdown of TCO_2 during spring through summer and by the upwelling of CO_2 -rich deep waters during fall through winter. Hence the CO_2 system in this area depends only weakly on the seawater temperature. This accounts for the highly variable coherence between $p\text{CO}_2$ and SST, and the 0.2 cpd peak which may represent the effects of wind-induced deep mixing events.

5. Summary and Conclusions

[26] A global database containing mainly underway measurements of surface water $p\text{CO}_2$ is used to estimate the spatial autocorrelation structure on a 10° latitude-longitude grid. Since the $p\text{CO}_2$ is a sensitive function of temperature and the total CO_2 concentration in seawater, which depends on biological utilization and upwelling of CO_2 -rich subsurface waters, its variability reflects both physical as well as biological processes. The $p\text{CO}_2$ is more densely sampled in space and time in the Northern Hemisphere than the Southern Hemisphere. The longest spatial correlations occur in the equatorial Pacific where the autocorrelations are above 0.8 out to distances between 80–100 km. The other equatorial areas also have relatively long correlation scales compared to other areas of the globe. The North Atlantic subtropical gyre has spatial correlation scales that tend to be about double the correlation scales in the subtropical gyre associated with the Kuroshio. This geographic distribution is similar to the distribution of the values of the first baroclinic Rossby radii of deformation as calculated by Emery *et al.* [1984], indicating that the physical properties of the flow field are a likely contributor to factors controlling the correlation scales. In the Indian Ocean, the correlation scales in the Southern Hemisphere tend to be longer than those in the Northern Hemisphere. A possible explanation for this variability can again be related to the controlling mechanisms of the flow field. An important mode for the southern Indian Ocean variability stems from long annual Rossby waves that are generated on the eastern side of the basin and propagate westward. The northern half of the basin is much more reactive to the strong forcing of the monsoonal flows. The correlation scales tend to be shortest at higher latitudes, again consistent with the scales of the deformation radius, but there is an

indication that after an initial steep drop off of the autocorrelation, there is a slowing of the drop off between 0.8 and 0.6 in the northern Atlantic.

[27] An attempt to estimate the temporal correlation structure is made at the only geographic location with relatively long (longer than about 10 days) uninterrupted time series of $p\text{CO}_2$ data at OWS "P" in the eastern North Pacific. Eleven time series were used to calculate the correlation structure with highly variable results. Most of these time series indicated a significant drop in autocorrelation (0.5 and lower) after 1–2 days. Three of the time series contained a more gentle drop off in the temporal correlation, but after 5 days, the correlation was only about 0.5. There was no obvious seasonal dependence in the temporal autocorrelation structure. Indeed, two of the time series that were separated by a single day during the summer of 1978 produced a drastically different autocorrelation structure from each other.

[28] The coherence of the geographic distribution of the spatial autocorrelation structures with physical properties of the flow, such as the internal Rossby radius of deformation, is encouraging. As assimilation models are contemplated for $p\text{CO}_2$, it is necessary to have confidence in an error covariance model for the data being ingested. An autocorrelation function provides a good start, and the fact that some of the global variability can be related to other physical variables gives some hope that any analysis product will be of more use than the ingested data alone. However, the inability to estimate a temporal autocorrelation structure is troubling. Even at OWS "P" where time series data exist, a stable estimate of that correlation structure proved difficult. Long uninterrupted time series measurements at fixed locations, such as those being conducted near the Pacific equator and elsewhere using moored buoy $p\text{CO}_2$ systems by the NOAA group, will help to improve our understanding of temporal variability scale. The estimates of the spatial correlation structure ignored any time change along a particular track, yet those correlations remained high over long distances, which also means over a time period of more than a couple days. Although modeling studies may be useful as a first guess for estimating $p\text{CO}_2$ correlation structure, confident estimates will require more and targeted measurements over the entire globe.

[29] **Acknowledgments.** This research was sponsored by the Carbon Cycle Science research initiative within NASA's Science Mission. This research was funded through NASA's Carbon Cycle Science program as announced in NRA-00-OES-08. Takahashi and Sutherland are supported through NASA grant NAG 5-11357. We acknowledge the following groups of investigators who provided the data analyzed in this study: C. S. Wong (IOS/Canada), R. A. Feely (PMEL/NOAA), Rik Wanninkhof (AOML/NOAA), Y. Nojiri (NIES/Japan), N. Bates (BBSR/Bermuda), B. Tilbrook (CSIRO/Australia), and A. Watson (University of East Anglia/UK).

References

- Bates, N. R., T. Takahashi, D. W. Chipman, and A. H. Knap (1998), Variability of $p\text{CO}_2$ on diel to seasonal timescales in the Sargasso Sea near Bermuda, *J. Geophys. Res.*, *103*, 15,567–15,585.
- Boutin, J., et al. (1999), Satellite sea surface temperature: A powerful tool for interpreting in situ $p\text{CO}_2$ measurements in the equatorial Pacific Ocean, *Tellus, Ser. B*, *51*, 490–508.
- Cosca, C. E., R. A. Feely, J. Boutin, J. Etcheto, M. J. McPhaden, F. P. Chavez, and P. G. Strutton (2003), Seasonal and interannual CO_2 fluxes for the central and eastern equatorial Pacific Ocean as determined from $f\text{CO}_2$ -SST relationships, *J. Geophys. Res.*, *108*(C8), 3278, doi:10.1029/2000JC000677.

- Emery, W. J., W. G. Lee, and L. Magaard (1984), Geographic and seasonal distributions of Brunt-Väissälä frequency and Rossby radii in the North Pacific and North Atlantic, *J. Phys. Oceanogr.*, *12*, 528–537.
- Feely, R. A., R. Wanninkhof, W. McGillis, M.-E. Carr, and C. E. Cosca (2004), Effects of wind speed and gas exchange parameterization on the air-sea CO_2 fluxes in the equatorial Pacific Ocean, *J. Geophys. Res.*, *109*, C08S03, doi:10.1029/2003JC001896.
- Loukos, H., F. Vivier, P. P. Murphy, D. E. Harrison, and C. Le Quéré (2000), Interannual variability of equatorial Pacific CO_2 from temperature and salinity data, *Geophys. Res. Lett.*, *27*, 1735–1738.
- Murphy, P. P., Y. Nojiri, D. E. Harrison, and N. K. Larkin (2001), Scales of variability for surface $p\text{CO}_2$ in the Gulf of Alaska and Bering Sea: Toward a sampling strategy, *Geophys. Res. Lett.*, *28*, 1047–1050.
- Rienecker, M. M., C. N. K. Mooers, and A. R. Robinson (1987), Dynamical interpolation and forecast of the evolution of mesoscale features off northern California, *J. Phys. Oceanogr.*, *17*, 1189–1213.
- Takahashi, T., J. Olafsson, J. Goddard, D. W. Chipman, and S. C. Sutherland (1993), Seasonal variation of CO_2 and nutrients in the high-latitude surface oceans: A comparative study, *Global Biogeochem. Cycles*, *7*, 843–878.
- Takahashi, T., R. A. Feely, R. Weiss, R. H. Wanninkhof, D. W. Chipman, S. C. Sutherland, and T. T. Takahashi (1997), Global air-sea flux of CO_2 : An estimate based on measurements of sea-air $p\text{CO}_2$ difference, *Proc. Natl. Acad. Sci.*, *94*, 8292–8299.
- Takahashi, T., et al. (2002), Global sea-air CO_2 flux based on climatological surface ocean $p\text{CO}_2$, and seasonal biological and temperature effects, *Deep Sea Res., Part II*, *49*, 1601–1622.
- Wong, C. S., and Y.-H. Chan (1991), Temporal variations in the partial pressure and flux of CO_2 at ocean station P in the subarctic northeast Pacific Ocean, *Tellus, Ser. B*, *43*, 206–223.
-
- D. Adamec, Oceans Sciences Branch, NASA Goddard Space Flight Center, Greenbelt, MD 20771, USA.
- Z. Li, NASA Goddard Space Flight Center, Global Modeling and Assimilation Office (GMAO), Code 610.1, Building 33, Room 214A, Greenbelt, MD 20771, USA. (zhen.li@gsfc.nasa.gov)
- S. C. Sutherland and T. Takahashi, Lamont-Doherty Earth Observatory of Columbia University, Palisades, NY 10964, USA.